Control of DFIG Wind Turbine With Direct-Current Vector Control Configuration

Shuhui Li, *Senior Member, IEEE*, Timothy A. Haskew, *Senior Member, IEEE*, Keith A. Williams, and Richard P. Swatloski

***Abstract*—The doubly-fed induction generator (DFIG) wind turbine is a variable speed wind turbine widely used in the modern wind power industry. At present, commercial DFIG wind turbines primarily make use of the technology that was developed a decade ago. But, it is found in this paper that there is a limitation in the conventional vector control technique. This paper presents a direct-current vector control method in a DFIG wind turbine, based on which an integrated control strategy is developed for wind energy extraction, reactive power, and grid voltage support controls of the wind turbine. A transient simulation system using SimPowerSystem is built to validate the effectiveness of the proposed control method. The conventional control approach is compared with the proposed control technique for DFIG wind turbine control under both steady and gust wind conditions. The paper shows that under the dc vector control configuration, a DFIG system has a superior performance in various aspects.**

***Index Terms*—DC-link voltage control, direct-current vector control, doubly-fed induction generator (DFIG) wind turbine, grid voltage support control, maximum power extraction, reactive power control.**

I. Introduction

AT THE present time, wind turbines based on doubly-fed induction generators (DFIGs) are used in most large wind power plants in North America [1]. There are several reasons for using DFIG wind turbines; among those are possibilities to increase turbine energy capture capability, reduce stresses of the mechanical structure, diminish acoustic noise, and make the active and reactive power controllable for better grid integration [1], [2].

However, the energy captured and converted from the wind by a DFIG wind turbine depends strongly on how the wind turbine is controlled under variable wind conditions. Presently, commercial DFIG wind turbines mainly use the technology that was developed a decade ago [2]–[4] based on the standard decoupled $d-q$ vector control mechanism. This paper shows that there is a limitation in the conventional vector control approach for the grid-side converter of the DFIG wind turbine. The weakness is more evident when the converter operates beyond its linear modulation limit. This situation has also been reported recently by many studies in different applications. In [5], it is found through both theoretical and experimental studies that the conventional control technique is sensitive to model uncertainties. In [6]–[8], it is reported that wind farms periodically experience high unbalance and harmonic distortions that have resulted in a large number of trips. In [9], it is pointed out that it is difficult to tune PI parameters for the conventional vector control technique in a STATCOM application. In [10], it is pointed out that it is the critical to be able to estimate the grid system parameter changes so as to enhance the performance of the conventional control method for a microgrid application.

This paper develops a mechanism for improved control of a DFIG wind turbine under a direct-current vector control configuration. Then, based on the proposed control structure, the integrated DFIG system control is developed, including maximum wind power extraction control, reactive power control, and grid voltage support control. In the sections that follow, the paper first introduces the general configuration of a DFIG system and overall control structure in Section II. Then, Section III presents the direct-current and conventional standard vector control approaches for a DFIG grid-side converter (GSC). The control of the rotor-side converter (RSC) is presented in Section IV. Section V shows the control integration of the GSC and RSC for DFIG maximum power extraction, reactive power, and grid voltage support controls. Simulation studies are conducted in Section VI to compare the performance of DFIG wind turbine using the direct-current and traditional vector control configurations for steady and variable wind conditions. Finally, the paper concludes with the summary of the main points.

II. DFIG Mechanical/Electrical Systems and Integrated Controls

A DFIG wind turbine primarily consists of three parts: a wind turbine drive train, an induction generator, and a power electronic converter (Fig. 1) [2], [4]. In the wind turbine drive train, the rotor blades of the turbine catch wind energy that is then transferred to the induction generator through a gearbox. The induction generator is a standard, wound rotor induction machine with its stator windings directly connected to the grid and its rotor windings connected to the grid through a frequency converter. The frequency converter is built by two self-commutated voltage-source converters, the RSC and the GSC, with an intermediate dc voltage link.

The control in a DFIG wind power plant has three levels: the generator level, the wind turbine level, and the wind power

Manuscript received June 08, 2010; revised March 06, 2011; accepted August 20, 2011. Date of current version December 16, 2011. This work was supported in part by the U.S. National Science Foundation under Grant CNS 1059265 and Grant ECCS 1102038.

S. Li and T. A. Haskew are with the Department of Electrical and Computer Engineering, The University of Alabama, Tuscaloosa, AL 35487 USA (e-mail: sli@eng.ua.edu).

K. A. Williams is with the Department of Mechanical Engineering, The University of Alabama, Tuscaloosa, AL 35487 USA.

R. P. Swatloski is with the Office for Technology Transfer, The University of Alabama, Tuscaloosa, AL 35487 USA.

Color versions of one or more of the figures in this paper are available online at http://ieeexplore.ieee.org.

Digital Object Identifier 10.1109/TSTE.2011.2167001

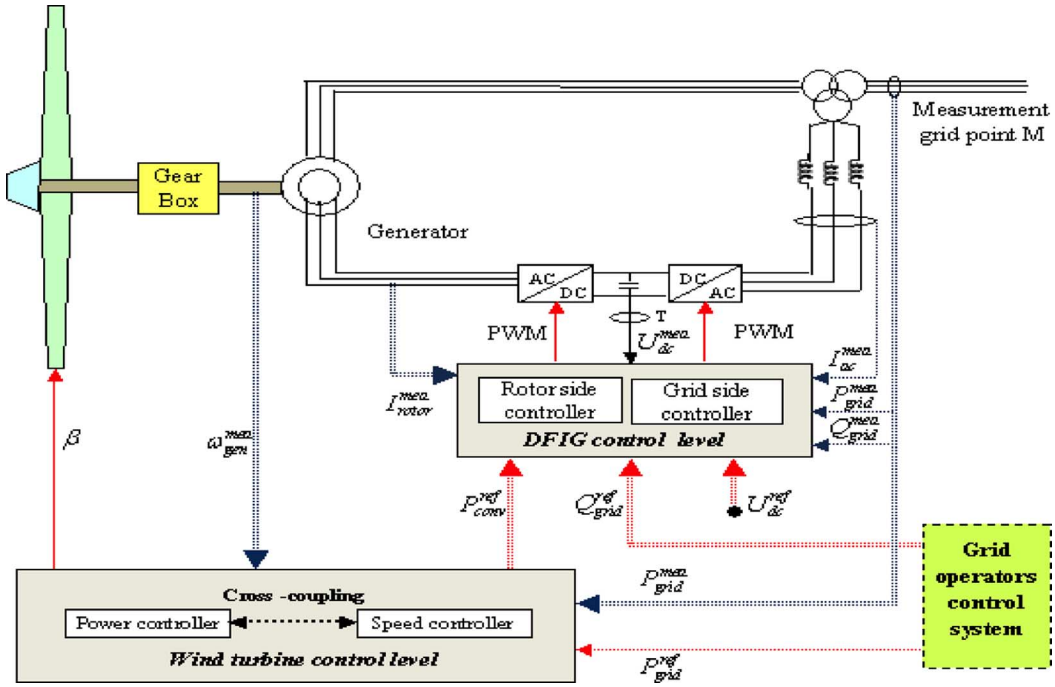

Fig. 1. Configuration of a DFIG system.

plant level (Fig. 1) [4]. At the generator level, the RSC controller regulates the DFIG to achieve one of the following two goals: 1) maximum energy extraction from the wind or 2) compliance with a wind plant control demand; the GSC controller maintains a constant dc-link voltage and adjusts reactive power absorbed from the grid by the GSC. At the turbine level, there are a speed controller and a power limitation controller. At a low wind speed, the speed controller gives a power reference to the RSC based on the principle of maximum energy extraction. At a high wind speed, the power limitation controller increases or decreases the pitch angle of the turbine blades to prevent the wind turbine from going over the rated power. At the wind power plant level, the power production of the entire plant is determined based on a grid requirement. The central control system sends out power references to each individual turbine, while the local turbine control system ensures that the power reference from the central control level is reached.

III. Conventional and Direct-Current Vector Control of GSC

In a DFIG wind turbine, the GSC controls the dc-link voltage and contributes to the reactive power or grid voltage support control of the overall DFIG system as well.

A. GSC Transient and Steady-State Models

Fig. 2 shows the schematic of the GSC, in which a dc-link capacitor is on the left and a three-phase voltage source, representing the voltage at the point of common coupling (PCC) of the ac system, is on the right.

In the $d-q$ reference frame, the voltage balance across the grid filter is

$$\begin{bmatrix} v_d \\ v_q \end{bmatrix} = R_f \begin{bmatrix} i_d \\ i_q \end{bmatrix} + L_f \frac{d}{dt} \begin{bmatrix} i_d \\ i_q \end{bmatrix} + \omega_s L_f \begin{bmatrix} -i_q \\ i_d \end{bmatrix} + \begin{bmatrix} v_{d1} \\ v_{q1} \end{bmatrix} \quad (1)$$

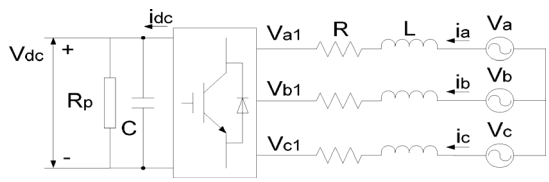

Fig. 2. Grid-connected converter schematic.

where ω_s is the angular frequency of the PCC voltage, and L_f and R_f are the inductance and resistance of the grid filter. Using space vectors, (1) is expressed by a complex (2) in which v_{dq}, i_{dq}, and v_{dq1} are instantaneous space vectors of the PCC voltage, line current, and converter output voltage. In the steady-state condition, (2) becomes (3), where V_{dq}, I_{dq}, and V_{dq1} stand for the steady-state space vectors of PCC voltage, grid current, and converter output voltage

$$v_{dq} = R_f \cdot i_{dq} + L_f \frac{d}{dt} i_{dq} + j\omega_s L_f \cdot i_{dq} + v_{dq1} \quad (2)$$

$$V_{dq} = R_f \cdot I_{dq} + j\omega_s L_f \cdot I_{dq} + V_{dq1}. \quad (3)$$

In the PCC voltage oriented frame [3], [11], the instant active and reactive powers absorbed by the GSC from the grid are proportional to grid d- and q-axis currents, respectively, as shown by (4) and (5)

$$p(t) = v_d i_d + v_q i_q = v_d i_d \quad (4)$$

$$q(t) = v_q i_d - v_d i_q = -v_d i_q. \quad (5)$$

In terms of the steady-state condition, $V_{dq} = V_d + j0$ if the d-axis of the reference frame is aligned along the PCC voltage position. Assuming $V_{dq1} = V_{d1} + jV_{q1}$ and neglecting the grid filter resistance, then, the current flowing between the PCC and the GSC according to (3) is

$$I_{dq} = (V_d - V_{d1})/(jX_f) - V_{q1}/X_f \quad (6)$$

in which X_f stands for the grid filter reactance.

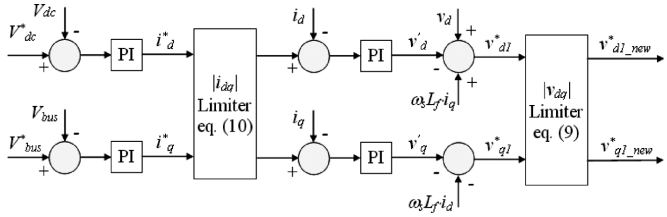

Fig. 3. Conventional standard GSC vector control structure.

Supposing passive sign convention is applied, i.e., power flowing toward the GSC as positive, then, the power absorbed by the GSC at the PCC is

$$P_{\text{conv}} = -V_d V_{q1}/X_f, \quad Q_{\text{conv}} = V_d(V_d - V_{d1})/X_f. \tag{7}$$

B. Conventional GSC Control Mechanism

The conventional vector control method for the GSC has a nested-loop structure consisting of a faster inner current loop and a slower outer loop, as shown by Fig. 3 [3], [4], [11], in which the d-axis loop is used for dc-link voltage control and the q-axis loop is used for reactive power or grid voltage support control. The control strategy of the inner current loop is developed by rewriting (1) as

$$v_{d1} = -(Ri_d + L \cdot di_d/dt) + \omega_s L i_q + v_d \tag{8}$$
$$v_{q1} = -(Ri_q + L \cdot di_q/dt) - \omega_s L i_d \tag{9}$$

in which the item in the bracket of (8) and (9) is treated as the transfer function between input voltage and output current for d and q loops, and the other terms are treated as compensation items [3], [4], [11]. This treatment assumes that v_{d1} in (8) has no major influence to $i_{\boldsymbol{q}}$ and v_{q1} in (9) has no main effect to i_d.

However, this assumption is inadequate as explained below. According to Fig. 3, the final control voltages v^*_{d1} and v^*_{q1}, linearly proportional to the converter output voltages V_{d1} and V_{q1} [12], include the d and q voltages v'_d and v'_q generated by the current-loop controllers plus the compensation terms as shown by (10). Hence, this control configuration intends to regulate i_d and $i_{\boldsymbol{q}}$ using v'_d and v'_q, respectively. But, according to (7), (4), and (5), d-axis voltage is only effective for reactive power or $i_{\boldsymbol{q}}$ control, and q-axis voltage is only effective for active power or $i_{\boldsymbol{d}}$ control. Thus, the conventional control method relies mainly on the compensation terms rather than the PI loops to regulate the d- and q-axis currents via a competing control strategy. Nevertheless, those compensation terms are not contributed in a feedback control principle

$$v^*_{d1} = -v'_d + \omega_s L_f i_q + v_d$$
$$v^*_{q1} = -v'_q - \omega_s L_f i_d. \tag{10}$$

The following issues are considered in the design of the conventional nested-loop control system.

1) To prevent the converter from getting into the nonlinear modulation mode, a saturation mechanism is applied to the output voltage of the controller if the amplitude of the reference voltage generated by the inner current-loop controller exceeds the converter linear modulation limit. The general strategy is to set a limitation on $|v^*_{dq1}|$ but keeps $\angle v^*_{dq1}$ unchanged as shown by (11) [13], [14], where $v^*_{d1\_\text{new}}$ and $v^*_{q1\_\text{new}}$ are the d and q components of the modified controller output voltage and $V_{\max}$ is the maximum allowable dq voltage. It is found that any other saturation mechanisms could cause more system oscillations and unbalances

$$v^*_{d1\_\text{new}} = V_{\max} \cdot \cos(\angle v^*_{dq1})\ v^*_{q1\_\text{new}} = V_{\max} \cdot \sin(\angle v^*_{dq1}). \tag{11}$$

2) To prevent the GSC from exceeding the rated current, the q-axis current reference is adjusted if the amplitude of the reference current generated by the outer control loop exceeds the rated current limit. The general approach is keeping the d-axis current reference i^*_d unchanged to maintain dc-link voltage control effectiveness while modifying the q-axis current reference i^*_q to satisfy the reactive power or ac bus voltage support control demand as much as possible as shown by (12) [13], [14]

$$i^*_{d\_\text{new}} = i^*_d\ \ i^*_{q\_\text{new}} = \text{sign}(i^*_q) \cdot \sqrt{(i^*_{dq\_\max})^2 - (i^*_d)^2}. \tag{12}$$

C. Direct-Current Vector Control of GSC

The theoretical foundation of the direct-current vector control approach for the GSC is (4) and (5), i.e., using d- and q-axis currents for active and reactive power control. But, unlike the conventional approach that generates a d- or q-axis voltage from a GSC current-loop controller, the direct-current vector control structure outputs a current signal at d or q current-loop controller. In other words, the output of the controller is a d or q tuning current while the input error signal tells the controller how much the tuning current should be adjusted during the dynamic control process. The development of the tuning current control strategy has adopted typical intelligent control concepts, i.e., a control goal to minimize absolute or root-mean-square (rms) error between the desired and actual d- and q-axis currents through an adaptive tuning mechanism [15]. This tuning current is different from the actual measured d or q current. For example, for a d-axis current reference, the adaptive tuning process would continue until the actual d-axis current reaches the d-axis reference current. It is necessary to point out that a fast current-loop controller is critical to assure the highest power quality in terms of harmonics and unbalance for the GSC [16]. Thus, elimination of the current control loop [17] is not an option for the proposed control design.

But, due to the nature of a voltage-source converter, the d- and q-axis tuning current signals i'_d and i'_q generated by the current-loop controllers must be transferred to d- and q-axis voltage signals v^*_{d1} and v^*_{q1} to control the GSC. This is realized through (13), which is equivalent to the transient $d-q$ (1) after being processed by a low-pass filter for the purpose of reducing the high oscillation of d and q reference voltages applied directly to the converter

$$v^*_{d1} = -R_f i'_d + \omega_s L_f i'_q + v_d$$
$$v^*_{q1} = -R_f i'_q - \omega_s L_f i'_d. \tag{13}$$

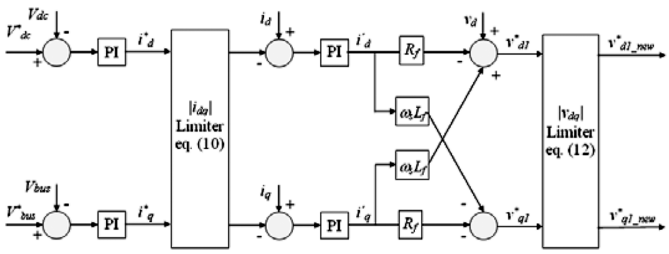

Fig. 4. GSC dc vector control structure.

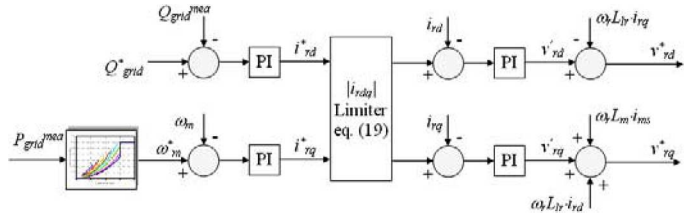

Fig. 5. DFIG speed and reactive power control structure of RSC.

The overall control structure of the GSC is shown by Fig. 4, which consists of a d-axis loop for dc-link voltage control and a q-axis loop for reactive power or grid voltage support control. Signal processing technology is applied to the measured dc-link voltage and d- and q-axis currents to prevent the high order harmonics from entering the controllers. The current-loop controller may integrate PI, fuzzy and adaptive control technologies to improve the dynamic performance of the GSC. The PI part of the controllers operates on a direct target control principle. The fuzzy and adaptive parts of the controllers adjust the PI parameters based on the error e, between the controlled variable and its target value, and the change in errorce [18]. The initial values of the PI current-loop controllers are tuned according to the fundamental intelligent control principle, i.e., minimizing the rms error between the reference and measured values [15].

In addition, a nonlinear programming strategy as shown below is utilized to prevent the GSC from going over the rated current and to avoid the converter getting into a nonlinear modulation mode, where $I_{\rm rated}$ is the rated GSC phase rms current and $Q^*_{\rm GSC}$ is the reference reactive power absorbed from the grid by the GSC. The basic principle of the nonlinear programming formulation is that under GSC rated current and linear modulation limits, the system should operate to achieve the dc-link voltage control goal while minimizing the difference between the reference and actual reactive power as much as possible

$$\begin{aligned}&\text{Minimize}: |Q_{\rm GSC}-Q^*_{\rm GSC}|\\ &\text{Subject to}: V_{\rm dc}=V^*_{\rm dc},\ \sqrt{(I_d^2+I_q^2)/3}\le I_{\rm rated},\\ &\qquad\qquad \sqrt{(V_{d1}^2+V_{q1}^2)/3}\le V_{\rm dc}/(2\sqrt{2}).\end{aligned}$$

The nonlinear programming strategy is implemented in the following way. If $|i^*_{dq}|$ generated by the outer dc-link voltage and reactive power control loops exceeds the rated current limit, i^*_d and i^*_q are modified by (12). If $|v^*_{dq1}|$ generated by the inner current control loops exceeds the converter linear modulation limit, the d- and q-axis voltages are recalculated by (14). As it can be seen, the recalculation does not change the q-axis control voltage v^*_{q1} so that the q-axis control loop is not affected. Hence, according to (7), the effectiveness of active power or dc-link voltage control is maintained. But, the recalculation makes the d-axis control voltage $v^*_{d1\_\rm new}$ does not follow the control voltage v^*_{d1} generated by the d-axis current-loop controller. Thus, the effectiveness of the reactive power or bus voltage support control, according to (7), would be affected. Under such conditions, the reactive power control is actually decided by the constraint of the converter linear modulation requirement but not the control rule

$$v^*_{d1\_\rm new}=\text{sign}(v^*_{d1})\cdot\sqrt{(v^*_{dq1\_\max})^2-(v^*_{q1})^2}\ \ v^*_{q1\_\rm new}=v^*_{q1}. \quad (14)$$

IV. RSC for DFIG Speed and Reactive Power Control

The RSC controls the induction generator of a DFIG wind turbine for energy extraction from the wind and coordinates with the GSC for reactive power or grid voltage support control of the overall DFIG system as well. The control is implemented through a nested-loop structure consisting of an inner current loop and an outer speed and reactive power loop [3], [4], [19]. Similar to the GSC, the importance of the RSC current control loop is to assure the highest power quality in terms of harmonics and unbalance for the DFIG. Hence, eliminating the current control [5]–[7] is not an option in this paper.

Fig. 5 shows the standard RSC control structure using the stator-flux oriented frame [2]–[4]. The direct-current vector control mechanism is not used because the rotor electrical frequency is near zero around the synchronous speed. In the figure, the speed reference is generated according to the maximum power extraction principle [4], [19] while the reactive power reference is generated based on a wind plant reactive power demand as well as the coordination of the reactive power control with the GSC (Section V). The reactive power reference is transferred to rotor d-axis current reference i^*_{rd} through a reactive-power controller and the torque reference, generated by the speed controller, is transferred to rotor q-axis current reference i^*_{rq}. The current-loop controllers generate d- and q-axis voltages, v'_{rd} and v'_{rq}, based on the error signals between the reference and actual rotor d- and q-axis currents. The final d- and q-axis control voltage, v^*_{rd} and v^*_{rq}, consists of the d- and q-axis voltage from the current-loop controllers, v'_{rd} or v'_{rq}, plus the compensation items as shown by Fig. 5.

In addition, to prevent the RSC from exceeding the rated current, the rotor d-axis current reference is adjusted by (15) if the amplitude of the reference current generated by the outer torque and reactive power control loops exceeds the rated rotor current limit. In fact, (15) represents a control rule of keeping i^*_{rq} unchanged to maintain wind power extraction effectiveness while modifying i^*_{rd} to meet the reactive power control demand as much as possible. The over modulation for the RSC is not a primary issue, which mainly happens beyond normal DFIG speed operating range [19]

$$i^*_{rd\_\rm new}=\text{sign}(i^*_{rd})\cdot\sqrt{(i^*_{rdq})^2-(i^*_{rq})^2}\ \ i^*_{rq\_\rm new}=i^*_{rq}. \quad (15)$$

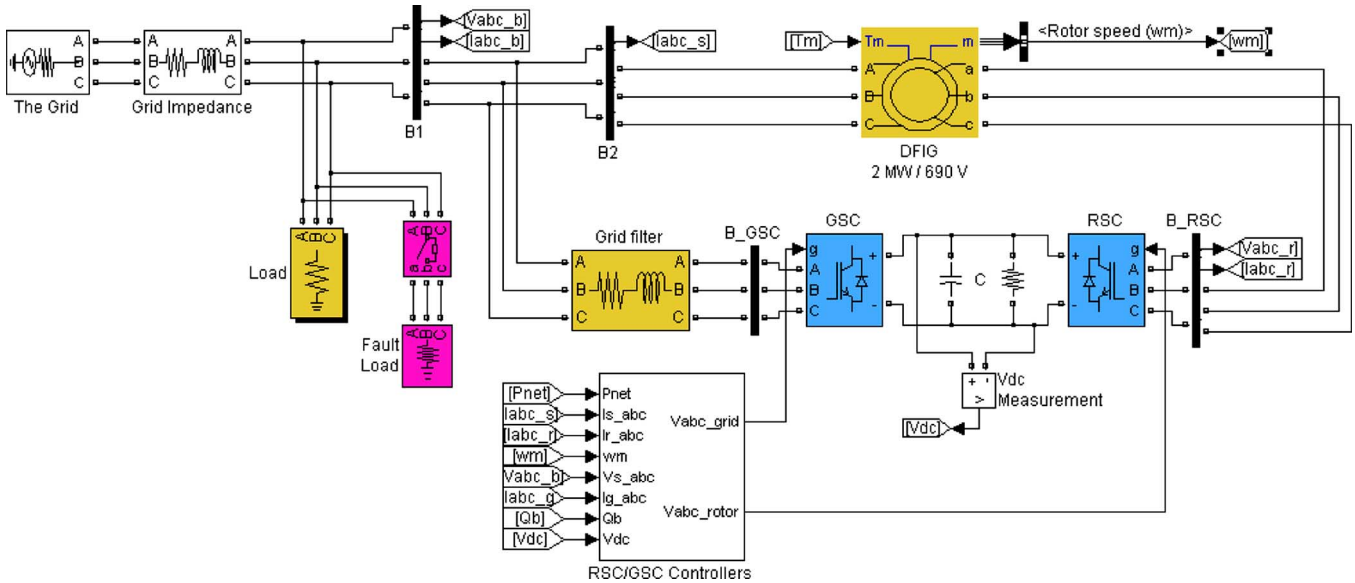

Fig. 6. GSC and RSC control of DFIG wind turbine in SimPowerSystems.

V. GSC and RSC for Integrated Wind Turbine Control

The key requirements for integrated DFIG wind turbine control include 1) maximum wind power extraction control, 2) reactive power control, and 3) grid voltage support control.

A. Maximum Wind Power Extraction Control

For a given wind speed, the goal of the maximum power extraction is to regulate the turbine rotating speed to an optimal speed so that the maximum power can be captured from the wind. The existing commercial technology, adopted in this paper, uses wind turbine output power and a $P-\omega$ lookup table for maximum power extraction design in a DFIG wind turbine [4]. This peak power tracking algorithm generates a speed reference to the speed-loop controller recursively until a maximum power extraction speed point is reached [20].

B. Reactive Power Control

As shown in Sections III and IV, both GSC and RSC can contribute to the reactive power control. In developing a coordinated reactive power control mechanism under the direct-current vector control configuration, the following strategies are employed. 1) The GSC contributes a part of the reactive power control demand while the RSC meets the rest reactive power control requirement. 2) The control objective of the GSC is to maintain a constant reactive power production while the control objective of the RSC is to assure that the overall reactive power production of the wind turbine meets the grid reactive power demand. 3) If the GSC reaches its physical constraints due to a high power transferred from DFIG rotor to the grid via the GSC, the converter is operated by maintaining the dc-link voltage constant as the first priority while meeting GSC reactive power control demand as much as possible as shown in Section IV-C. Under this condition, the GSC may absorb reactive power so that the RSC must generate reactive power to meet both the GSC and wind plant reactive power demand. But, this control mechanism cannot be applied to the conventional GSC control structure (Fig. 3), which could result in high oscillations and unbalances of the overall system due to its competing control nature (Section III-B).

C. PCC Voltage Support Control

A fault of the ac power system usually causes the PCC voltage to drop. Like a conventional synchronous generator, it is preferred that a DFIG wind turbine should have certain voltage support ability. During a voltage sag of the ac system, the GSC, similar to a STATCOM, should generate a reactive power as much as possible. The design strategies for integrated GSC and RSC voltage support control under the direct-current vector control structure are the following. 1) The GSC, operating as a STATCOM [21], should provide the voltage support control capability as much as possible. 2) The control objective of the GSC is to contribute to a part of the voltage support task while the control objective of the RSC is to meet the rest of the voltage support requirement. 3) If the GSC and/or RSC reach the physical constraints of the converters, the system should operate by maintaining the dc-link voltage constant as the first priority from the GSC standpoint and by preserving the maximum power extraction control as the primary concern from the RSC perspective.

Nevertheless, if using the traditional standard control structure for the GSC, the speed of GSC voltage support controller must be much slower than that of the RSC voltage support controller. Otherwise, it would be very easy for the GSC controller to generate a control voltage that is over the converter linear modulation limit and, therefore, influence the stability of the overall DFIG system, as shown in Section VI-B. This situation would limit the ability of the GSC to function as a STATCOM during the voltage support control mode.

VI. Control Evaluation and Comparison

To evaluate and compare the peak power tracking, reactive power, and grid voltage support controls using the conventional and direct-current vector control approaches, an integrated

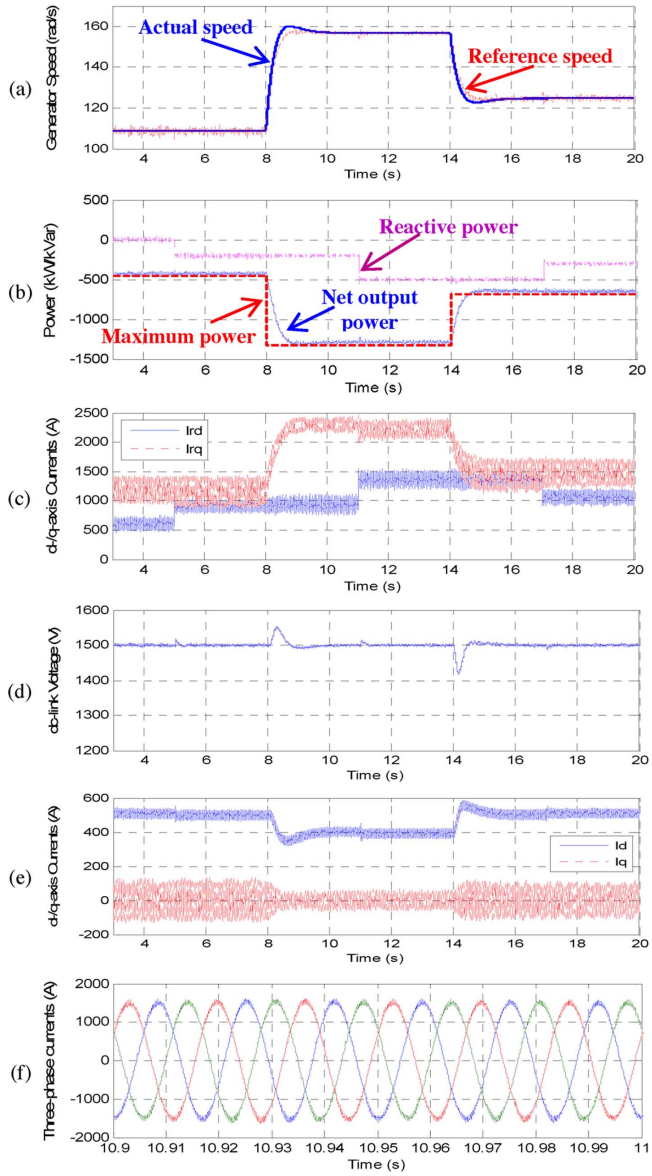

Fig. 7. GSC and RSC for maximum power extraction and reactive power controls using conventional control method (steady wind).

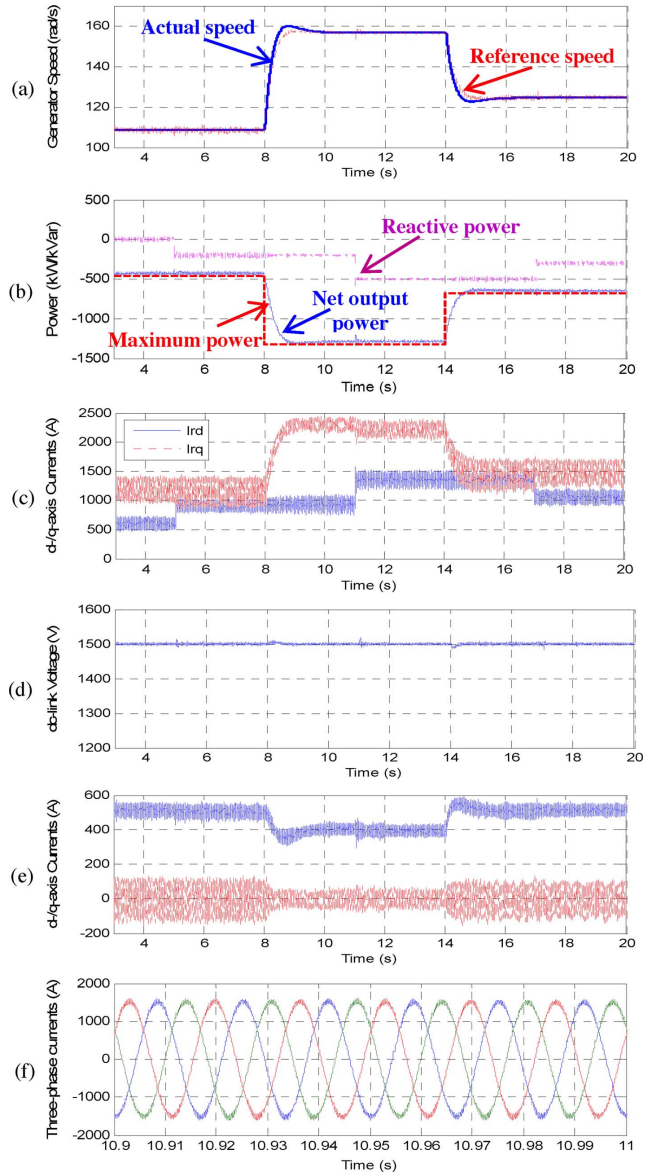

Fig. 8. GSC and RSC for maximum power extraction and reactive power controls using proposed control method (steady wind).

transient simulation system of a DFIG system is developed by using power converter average and detailed switching models in MatLab SimPowerSystems, in which both steady and variable wind conditions are considered. The average model is used for an initial evaluation while the detailed switching model (Fig. 6) is used for more practical investigation. For the switching-model based DFIG system, losses within the power converters and dc-link capacitor are considered. The system parameters are shown in Tables I and II in the Appendix. The grid impedance is the equivalent impedance referred to a DFIG wind turbine by considering the effect of 100 wind turbines operating at the same condition [22], [23]. The converter switching frequency is 1980 Hz for both GSC and RSC. All the results presented in this paper are based on the switching-model simulation.

A. Peak Power Tracking and Reactive Power Control

Figs. 7 and 8 present a case study of peak power tracking and reactive power control under a steady wind condition using the traditional and proposed vector control approaches, respectively. The q-axis current reference of the GSC controller is set to zero so that the wind plant reactive power demand is met by the RSC control. Before $t = 4$ s, the wind speed is 7 m/s and the reactive power reference is 0 kVar. After the system is stable, the output power of the wind turbine is very close to the maximum power that can be captured by the turbine at this wind speed [Figs. 7(b) and 8(b)]. The net reactive power is maintained at the reactive power reference, and the dc-link voltage is stabilized at the desired dc voltage reference of 1500 V [Figs. 7(d) and 8(d)]. At $t = 5$ s when the grid reactive power demand changes to -200 kVar (generating), the net reactive power of the wind turbine quickly gets to the new reactive power reference [Figs. 7(b) and 8(b)]. At $t = 8$ s, as the wind speed changes from 7 to 10 m/s, the peak power tracking strategy recursively generates reference generator speed [Figs. 7(a) and 8(a)] while the control of the RSC regulates the generator speed and turbine output power smoothly

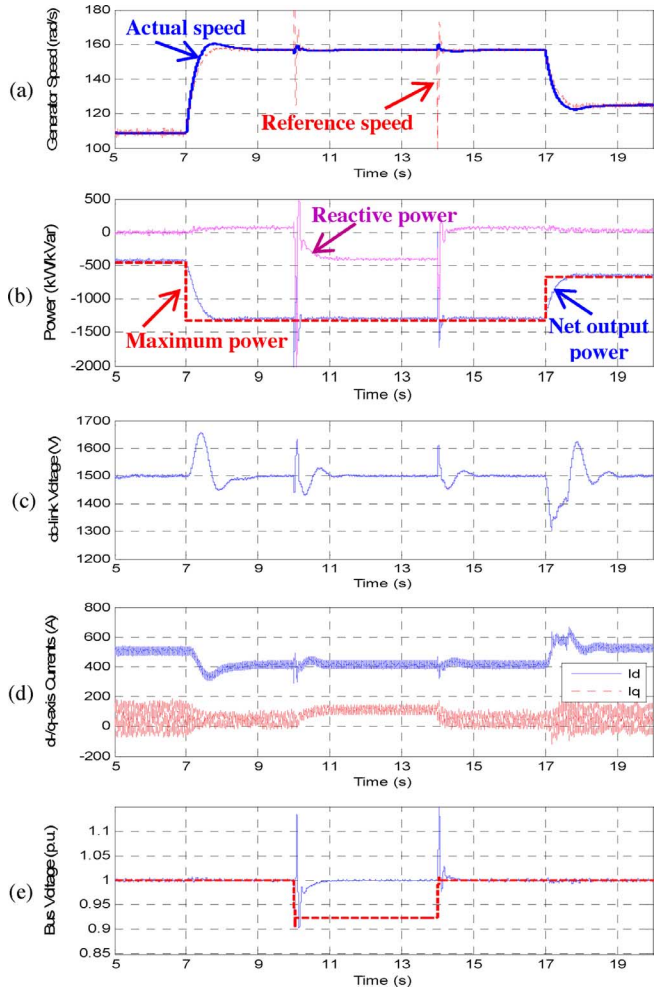

Fig. 9. GSC and RSC for maximum power extraction and voltage support controls during a low voltage droop (conventional approach).

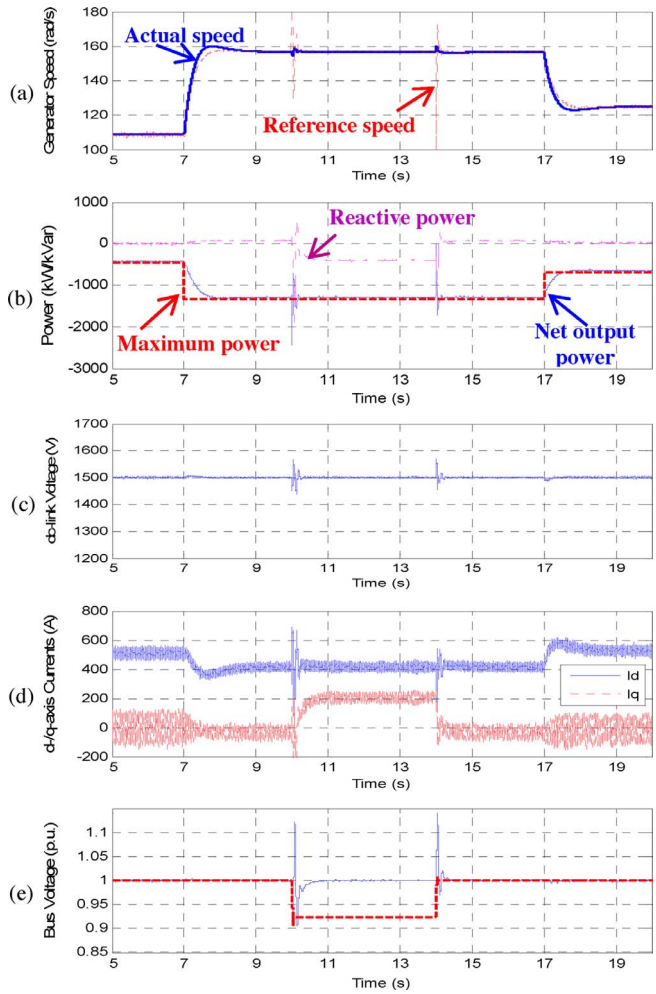

Fig. 10. GSC and RSC for maximum power extraction and voltage support controls during a low voltage droop (proposed approach).

until the new maximum power point is reached. With more power captured from the wind under a higher wind speed, the instantaneous rotor q-axis current i_{rq} increases [Figs. 7(c) and 8(c)] but the generator speed shifts closer to the synchronous speed [Figs. 7(a) and 8(a)]. This causes the power absorbed by the rotor to decrease [24], GSC d-axis current to drop [Figs. 7(e) and 8(e)], and the dc-link voltage to increase. Compared to the traditional control method [Fig. 7(d)], the direct-current vector control of the GSC stabilizes the dc-link voltage much faster [Fig. 8(d)], showing the superior performance of the system under the direct-current vector control configuration. For other reactive power demand changing from -200 to -500 kVar at $t = 11$ s and from -500 to -300 kVar at $t = 17$ s, and a wind speed variation from 10 to 8 m/s at $t = 14$ s, the integrated GSC and RSC control under the direct-current vector control structure performs effectively for maximum power extraction, reactive power, and dc-link voltage controls with the three-phase current transferred between the grid and the DFIG having a high power quality that is equivalent to the conventional standard control method [Figs. 7(f) and 8(f)].

B. Peak Power Tracking and Voltage Support Control

In voltage support control mode, both d- and q-axis current references of the GSC controller are variable, making $|v^*_{dq1}|$ generated by the controller more possible to go over the converter linear modulation limit. This situation presents a challenge to the conventional GSC control method. In order to make the DFIG system stable during the voltage support control mode, the speed of the dc-link voltage controller must be slow by retuning the PI coefficients. But, for the direct-current vector control configuration, the PI coefficients remain unchanged, showing superior adaptability of the direct-current control mechanism to different control conditions. Figs. 9–12 present a PCC voltage support control study for low and high voltage sag conditions, respectively. In all the figures, a voltage droop is generated between 10 and 14 s. The wind speed is 7 m/s before 7 s, 10 m/s from 7 to 17 s, and 8 m/s after 17 s.

For a low voltage sag on the PCC bus, the integrated GSC and RSC control under the direct-current vector control configuration works properly for peak power tracking [Fig. 10(b)], dc-link voltage [Fig. 10(c)], and the PCC bus voltage support control [Fig. 10(e)]. At the start of the voltage sag, there is a sudden change of the rotor $d - q$ current [25], which results in a sharp fluctuation of dc-link voltage, PCC bus voltage, wind turbine output power, and the reference speed generated by the P-ω lookup table (Fig. 10). But, the integrated GSC and RSC control under the direct-current vector control configuration quickly stabilize the dc-link voltage and recover the

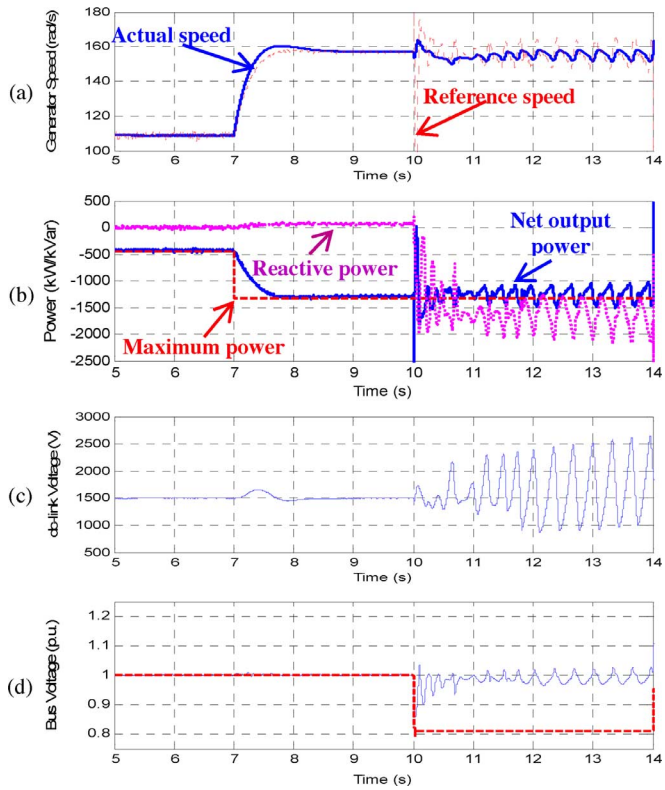

Fig. 11. GSC and RSC for maximum power extraction and voltage support control during a moderate voltage droop (conventional approach).

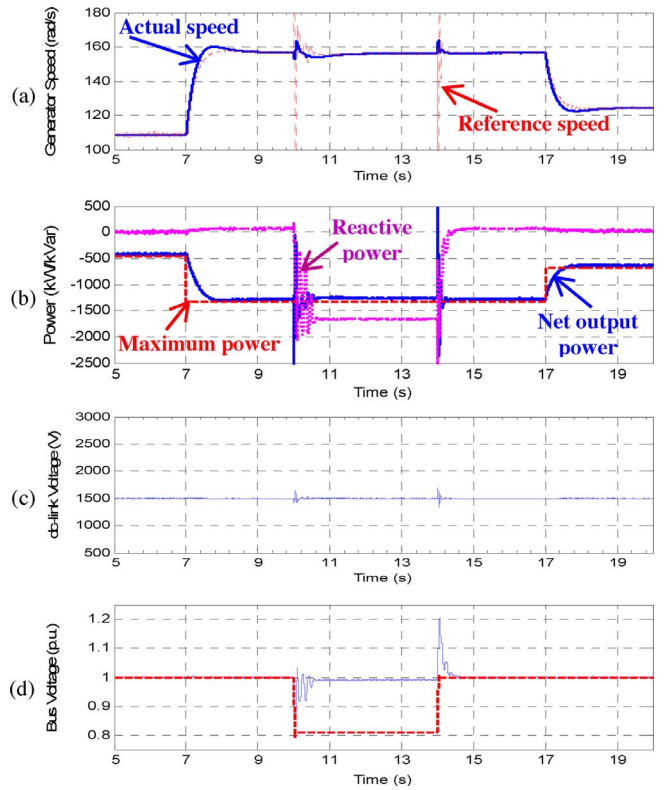

Fig. 12. GSC and RSC for maximum power extraction and voltage support controls during a moderate voltage droop (proposed approach).

PCC bus voltage to the rated value. During the voltage support control mode, the GSC, operating as a STATCOM, increases q-axis current i_q until the rated current or linear modulation constraint of the GSC is reached [Fig. 10(d)]. When the voltage sag is cleared at 14 s, there is another oscillation of the PCC voltage. Again, the integrated GSC and RSC control under the direct-current vector control configuration quickly recover the DFIG system to the normal operation.

For the conventional control method, more oscillation of the dc-link voltage is found as shown by Fig. 9(c) due to a slow dc-link voltage controller that is necessary to assure stable DFIG operation during the voltage support control mode. Even so, it is found that the system is still very fragile to get into an unstable state for any small disturbance using the conventional control approach.

For a moderate voltage sag on the PCC bus, the direct-current vector control strategy again is able to manage the control task properly as shown by Fig. 12. However, more oscillations are found on the rotor $d-q$ current. Although the fluctuation of the reference speed generated by the P-ω lookup table is higher, the change of the generator speed is small due to a large wind turbine inertia. Compared to a low voltage sag condition, more generating reactive power is needed to boost the PCC bus voltage. But, due to the rated current or converter linear modulation constraints of both the GSC and RSC, the total reactive power generated by the GSC and RSC cannot meet the reactive power demand for the voltage support control [Fig. 12(b)]. Thus, the final PCC bus voltage after the voltage support control is a little bit less than the rated PCC bus voltage of 1 pu [Fig. 12(d)]. In general, under a moderate voltage sag condition, the integrated GSC and RSC control performs well for maximum power extraction, dc-link voltage, and PCC bus voltage support control under the direct-current vector control configuration.

For the conventional control method, however, the system would get into a malfunction state when the output voltage of the GSC controller exceeds the converter linear modulation limit, during which high oscillations are found in the DFIG system and the system losses its stability after the voltage sag is cleared at $t = 14$ s (Fig. 11). This situation has also been reported by several recent studies in wind power, which indicates that wind farms periodically experience high unbalance and harmonic distortions that have resulted in a large number of trips [21]–[23]. But, the study of this paper implies that those abnormal operations may be caused by the malfunction of the conventional standard GSC vector control approach under special conditions.

C. GSC and RSC Control Under Variable and Gust Wind

In reality, wind speed changes constantly over time. Over periods shorter than an hour, wind speed can be approximated as the superposition of a slowly varying mean speed V_w plus N sinusoidal components having frequencies ω_i, amplitudes A_i, and random phases ϕ_i, as shown by (16) [25]

$$v_w(t) = V_w + \sum_{i=1}^{N} A_i \cos(\omega_i t + \phi_i). \tag{16}$$

In (16), ω_i is a random variable that has Von Karman distribution described by (17), where L represents the roughness of the

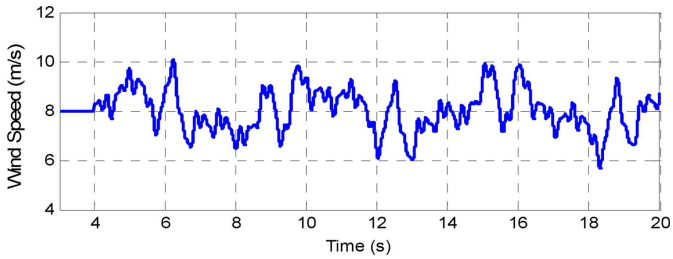

Fig. 13. Illustration of a variable wind speed.

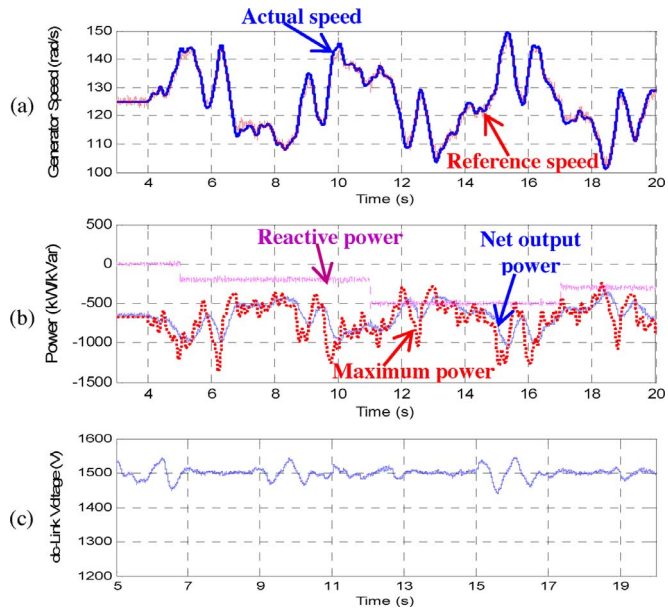

Fig. 14. GSC and RSC for maximum power extraction and voltage support controls during a moderate voltage droop (conventional approach).

area around the wind turbine and σ is the standard deviation of the wind speed distribution. The amplitude A_i of each discrete frequency component, chosen to give it a power equal to that contained in a certain frequency band, is calculated by (18) [25]

$$S_{vv}(\omega_i) = \frac{0.475\sigma^2(L/V_w)}{[1+(\omega_i L/V_w)^2]^{5/6}} \tag{17}$$

$$A_i(\omega_i) = \sqrt{(S_{vv}(\omega_i)+S_{vv}(\omega_{i+1}))(\omega_{i+1}-\omega_i)}. \tag{18}$$

Using (16)–(18), a variable and gust wind condition is generated as shown by Fig. 13. Before $t = 4$ ms, the wind speed is 8 m/s. The variable and gust wind starts at $t = 4$ s with $V_w = 8$ m/s. Figs. 14 and 15 compare the performance of the integrated GSC and RSC control for peak power tracking and reactive power control using the traditional and proposed control approaches under the variable and gust wind condition while the rest conditions are the same as those used in Figs. 7 and 8. Due to the oscillating wind speed, the maximum available power that can be extracted by a DFIG wind turbine fluctuates sharply. However, the turbine rotating speed and the net output power shift smoothly using the recursive lookup table peak power tracking control strategy (Figs. 14 and 15). The net output power of the wind turbine follows the maximum available power properly while the influence of the gust wind is

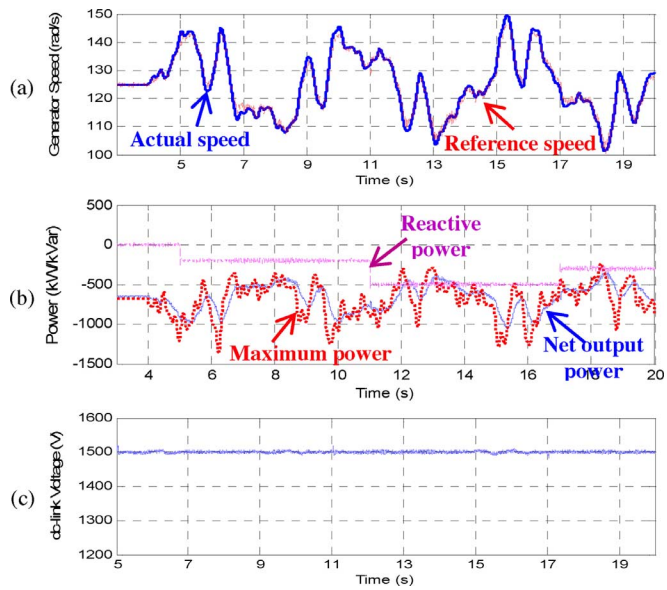

Fig. 15. GSC and RSC for maximum power extraction and voltage support controls during a moderate voltage droop (proposed approach).

restrained as shown by Figs. 14(b) and 15(b), demonstrating the effectiveness and stability of the recursive peak power tracking control mechanism in variable and gust wind conditions. The variation of the wind speed causes a fluctuating active power transferred from the rotor to the grid through the GSC. But, using the direct-current vector control configuration, the dc-link voltage is properly maintained around the reference voltage with very small fluctuation [Fig. 15(c)]. Nevertheless, if using the conventional standard control approach, the oscillation of the dc-link voltage is more evident [Fig. 14(c)].

VII. Conclusion

This paper presents a DFIG wind turbine control study using a direct-current vector control design. The paper compares the proposed control scheme with the conventional standard DFIG control method. The paper shows under the direct-current vector control configuration, how the integrated GSC and RSC control is designed to implement the maximum power extraction, dc-link voltage, reactive power, and grid voltage support control functions.

Comprehensive simulation studies demonstrate that the proposed DFIG wind turbine control structure can effectively accomplish wind turbine control objectives with superior performance under both steady and variable wind conditions within physical constraints of a DFIG system. Beyond physical constraints of a DFIG system, the proposed control approach operates the system by regulating the RSC for maximum wind power extraction as the first priority and by controlling the GSC to stabilize the dc-link voltage as the main concern.

The direct-current vector current structure is also effective for peak power tracking and grid voltage support control under a low voltage sag condition. But, for a high PCC bus voltage sag, it may be impossible to boost the PCC voltage to the rated voltage because of the rated current and converter linear modulation constraints.

Compared to the conventional standard DFIG control approach, the proposed method is more stable and reliable, has better dynamic performance, and demonstrates superior behavior particularly under the ac system bus voltage control mode.

APPENDIX

TABLE I
PARAMETER OF DFIG WIND TURBINE

Parameter	Value	Units
S_g (Generator rated power)	2000	kVA
f (frequency)	60	Hz
V_g (Generator rated Voltage)	690	V
R_s (stator resistance)	0.0043	p.u.
X_{ls} (stator reactance)	0.0809	p.u.
R_r (rotor resistance referred to stator side)	0.0048	p.u.
X_{lr} (rotor reactance referred to stator side)	0.0871	p.u.
X_m (magnetizing reactance)	3.459	p.u.
C (dc-link capacitor)	16000	μF
R_f (grid-filter resistance)	0.012	Ω
L_f (grid-filter inductance)	2	mH

TABLE II
RELEVANT DATA OF A WIND POWER PLANT

Equipment	Voltage ratio	R (pu)	X (pu)	Base Power
Wind turbine transformer	0.69/36KV	0.8%	4.52%	2MW
PCC transformer	36/200KV	0.5%	6.5%	150MW
Transmission line	200KV	2.54%	11.9%	300MW
Grid transformer	200/400kV	0.024%	2.4%	150MW

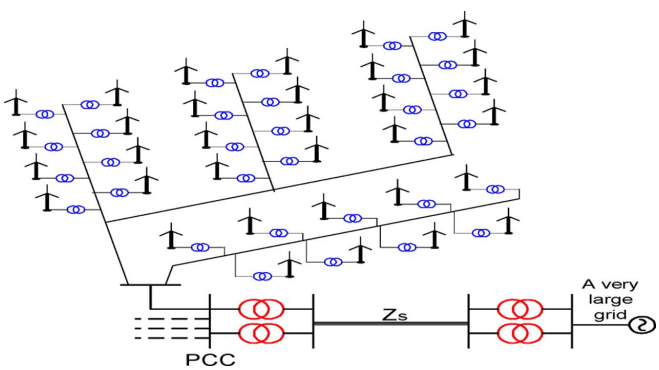

Fig. A1. Illustration of a wind power plant.

REFERENCES

[1] R. Zavadil, N. Miller, A. Ellis, and E. Muljadi, "Making connections: Wind generation challenges and progress," *IEEE Power Energy Mag.*, vol. 3, no. 6, pp. 26–37, Nov. 2005.

[2] S. Muller, M. Deicke, and R. W. De Doncker, "Doubly fed induction generator systems for wind turbines," *IEEE Ind. Appl. Mag.*, vol. 8, no. 3, pp. 26–33, May/Jun. 2002.

[3] R. Pena, J. C. Clare, and G. M. Asher, "Doubly fed induction generator using back-to-back PWM converters and its application to variable speed wind-energy generation," in *Proc. Inst. Elect. Eng., Elect. Power Appl.*, May 1996, vol. 143, no. 3.

[4] A. D. Hansen, P. Sørensen, F. Iov, and F. Blaabjerg, "Control of variable speed wind turbines with doubly-fed induction generators," *Wind Eng.*, vol. 28, no. 4, pp. 411–432, Jun. 2004.

[5] J. Dannehl, C. Wessels, and F. W. Fuchs, "Limitations of voltage-oriented PI current control of grid-connected PWM rectifiers with *LCL* filters," *IEEE Trans. Ind. Electron.*, vol. 56, no. 2, pp. 380–388, Oct. 2009.

[6] D. W. Zhi and L. Xu, "Direct power control of DFIG with, constant switching frequency and improved transient performance," *IEEE Trans. Energy Convers.*, vol. 22, no. 1, pp. 110–118, Mar. 2007.

[7] L. Xu and P. Cartwright, "Direct active and reactive power control of DFIG for wind energy generation," *IEEE Trans. Energy Convers.*, vol. 21, no. 3, pp. 750–758, Sep. 2006.

[8] L. Xu and Y. Wang, "Dynamic modeling and control of DFIG based wind turbines under unbalanced network conditions," *IEEE Trans. Power Syst.*, vol. 20, no. 1, pp. 314–323, Feb. 2007.

[9] A. Luo, C. Tang, Z. Shuai, J. Tang, X. Xu, and D. Chen, "Fuzzy-PI-based direct-output-voltage control strategy for the STATCOM used in utility distribution systems," *IEEE Trans. Ind. Electron.*, vol. 56, no. 7, pp. 2401–2411, Jul. 2009.

[10] J. C. Vasquez, J. M. Guerrero, A. Luna, P. Rodríguez, and R. Teodorescu, "Adaptive droop control applied to voltage-source inverters operating in grid-connected and islanded modes," *IEEE Trans. Ind. Electron.*, vol. 56, no. 10, pp. 4088–4096, Oct. 2009.

[11] A. Mullane, G. Lightbody, and R. Yacamini, "Wind-turbine fault ride-through enhancement," *IEEE Trans. Power Syst.*, vol. 20, no. 4, pp. 1929–1937, Nov. 2005.

[12] N. Mohan, Advanced Electric Drives—Analysis, Modeling and Control Using Simulink Minnesota Power Electronics Research & Education, MN, ISBN 0-9715292-0-5.

[13] R. Gagnon, Detailed Model of a Doubly-Fed Induction Generator (DFIG) Driven by a Wind Turbine The MathWork, Jan. 2006.

[14] P. Giroux and G. Sybille, Static Synchronous Compensator (STATCOM) Used for Midpoint Voltage Regulation on a 500 kV Transmission Line The MathWork, Jan. 2006.

[15] S. Haykin, *Neural Networks: A Comprehensive Foundation*. Englewood Cliffs, NJ: Prentice-Hall, 1999.

[16] J. C. Moreno, J. M. E. Huerta, R. G. Gil, and S. A. González, "A robust predictive current control for three-phase grid-connected inverters," *IEEE Trans. Ind. Electron.*, vol. 56, no. 6, pp. 1993–2004, Oct. 2009.

[17] A. Luo, C. Tang, Z. Shuai, J. Tang, X. Xu, and D. Chen, "Fuzzy-PI-based direct-output-voltage control strategy for the STATCOM used in utility distribution systems," *IEEE Trans. Ind. Electron.*, vol. 56, no. 7, pp. 2401–2411, Jul. 2009.

[18] S. Li, T. A. Haskew, and L. Xu, "Conventional and novel control designs for direct driven PMSG wind turbines," *Electric Power Syst. Res.*, vol. 80, no. 3, pp. 328–338, Mar. 2010.

[19] S. Li, T. A. Haskew, Y. Hong, and S. Mazari, "Integrating electrical and aerodynamic characteristics for DFIG wind energy extraction and control study," *Int. J. Energy Res.*, vol. 34, no. 12, pp. 1052–1070, Oct. 2010.

[20] S. Li, T. A. Haskew, and E. Muljadi, "DFIG maximum wind power extraction study through integrated steady-state and close-loop control evaluation," *Electric Power Compon. Syst. (Taylor & Francis)*, vol. 38, no. 7, pp. 767–785, 2010.

[21] E. Acha, C. R. Fuerte-Esquivel, H. Ambriz-Perez, and C. Angeles-Camacho, *FACTS—Modeling and Simulation in Power Networks*. Chichester, England: Wiley, 2004.

[22] E. Muljadi, Y. Wan, C. P. Butterfield, and B. Parsons, "A study of a wind farm power system," in *Proc. 21st American Society of Mechanical Engineers Wind Energy Symp.*, Reno, NV, Jan. 14–17, 2002.

[23] S. Li, T. A. Haskew, and R. Challoo, "Steady-state characteristic study for integration of DFIG wind turbines into transmission grid," *Int. J. Emerging Electric Power Syst.*, vol. 10, no. 1, Jan. 2009, Article 7, DOI: 10.2202/1553-779X.1967.

[24] A. D. Hansen and G. Michalke, "Fault ride-through capability of DFIG wind turbines," *Renew. Energy*, vol. 32, pp. 1594–1610, 2007.

[25] B. G. Rawn, P. W. Lehn, and M. Maggiore, "Control methodology to mitigate the grid impact of wind turbines," *IEEE Trans. Energy Convers.*, vol. 22, no. 2, pp. 431–438, Jun. 2007.

Shuhui Li (S'99–M'99–SM'08) received the B.S. and M.S. degrees in electrical engineering from Southwest Jiaotong University in Chengdu, China, in 1983 and 1988, respectively, and the Ph.D. degree in electrical engineering in 1999, from Texas Tech University.

From 1988 to 1995, he was with the School of Electrical Engineering, Southwest Jiaotong University, where his fields of research interest include modeling and simulation of large dynamic systems, dynamic process simulation of electrified railways, power electronics, power systems, and power system harmonics. From 1995 to 1999, he was engaged in research on wind power, artificial neural networks, and applications of massive parallel processing. He joined Texas A&M University–Kingsville as an Assistant Professor in 1999 and then as an Associate Professor in 2003. He worked with Oak Ridge National Laboratory for simulation system development on supercomputers in 2004 and 2006. He joined the University of Alabama as an Associate Professor in 2006. His current fields of interest include renewable energy systems, power electronics, power systems, electric machines and drives, FACTS, intelligent control, microgrids, and distributed generation.

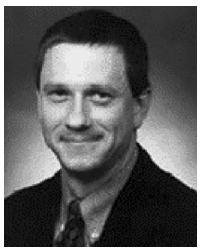

Timothy A. Haskew (S'86–M'87–SM'02) received the B.E.E., M.S., and Ph.D. degrees in electrical engineering from Auburn University in Auburn, AL, in 1987, 1988, and 1991, respectively.

He holds the rank of Professor of Electrical and Computer Engineering at the University of Alabama, Tuscaloosa, AL, where he serves as the Director of the Electromechanical Systems Laboratory and as the Electrical and Computer Engineering Graduate Program Director. He has been at the University of Alabama since 1991. His research interests include electromechanical systems, electric machinery, power electronics, and control systems.

Dr. Haskew is a member of the Power Electronics, Power and Energy, and Industry Applications societies of the IEEE. He has served on the program committee for the IEEE Applied Power Electronics Conference as the Seminar Chair and has authored or coauthored over 50 refereed publications and two book chapters.

Keith A. Williams received the B.S. degree in civil engineering from the University of Vermont in 1993 and the M.S. and Ph.D. degrees in mechanical engineering from Iowa State University and Purdue University in 1995 and 2001, respectively.

He is currently an Associate Professor of Mechanical Engineering at The University of Alabama, where he has been teaching since 2001. His research interests are in the areas of controls, dynamic systems, vibrations, and mechatronics. His past research has included work in the areas of fuel cell dynamic response, vibration control with shape memory alloys, and testing and modeling of the human vestibular system.

Dr. Williams is a member of ASME.

Richard P. Swatloski recived both the bachelor's and Ph.D. degrees in chemistry from the University of Alabama (UA).

In 2006, he accepted a position as a Licensing Associate and helped establish UA's Office for Technology Transfer. His current duties include various aspects of intellectual property protection, management and licensing, agreement development, new business creation, and education. He is also active in the Association for University Technology Managers (AUTM), serving on the planning committee for AUTM's Annual Eastern Regional Meeting.

Dr. Swatloski has received multiple awards and recognition, including the Kenneth G. Hancock Memorial Award for ionic liquid and green chemistry achievements. He has contributed to over 50 peer-reviewed publications and multiple patents. His work has been presented over 120 times at both national and international meetings, and he is recognized as a leading scientist in the field of ionic liquid chemistry.